An idealized model for tsunami study

Joshua Tobias[1] and Michael Stiassnie[1]

Received 26 October 2010; revised 1 March 2011; accepted 5 April 2011; published 29 June 2011.

[1] An idealized mathematical model of tsunami evolution in deep sea and across the continental shelf is proposed. The initial value problem in deep sea is related to the well-known Cauchy- Poisson problem and the tsunami propagation across the continental shelf is derived using the linearized shallow water equations. When analyzing different cases of tsunamis in deep sea, it was found that tsunamis evolve into two basic wave types. One resembles a single wave and the other a wave packet. The analysis of different cases of tsunamis at the shoreline reveals that the continental shelf, due to its geometrical properties, serves as a tsunami amplifier, producing tsunami amplitudes up to 20 times larger than those at the edge of the continental shelf. A comparison with tsunami measurements suggests that the idealized model may be used for a reliable assessment of the principle hydrodynamic properties of the tsunami, such as the tsunami amplitude and its half period.

Citation: Tobias, J., and M. Stiassnie (2011), An idealized model for tsunami study, *J. Geophys. Res.*, *116*, C06026, doi:10.1029/2010JC006763.

1. Introduction

[2] Tsunamis caused by earthquakes typically evolve from deep sea as extremely long waves with small steepness. By nature the tsunami consists of a number of transient and nonperiodic waves, and during the propagation from the deep sea to the nearshore area these waves gradually modify with respect to amplitudes, wavelengths, and wave periods. A major amplification of amplitude and flow velocity occurs during the last stages of shoaling and runup.

[3] Various numerical models using different approximations of the full hydrodynamic problem have been used to tackle this important phenomenon. For details the reader is referred to the recent book of *Levin and Nosov* [2009].

[4] Two recent papers, *Madsen et al.* [2008] and *Constantin and Henry* [2009], which have questioned the relevance of the Solitary wave paradigm for tsunamis, have encouraged us to investigate the quality of results produced by linearized tsunami models [see also *Hammack and Segur*, 1978]. The purpose of this study is to provide a simple, but meaningful, model for tsunami calculation. The goal is to provide a mostly analytical solution, based on as little as possible input parameters, which produce the dominant hydrodynamic features. Such a model enables new physical insight and may serve, for instance, to generate synthetic tsunami databases.

[5] The smallest number of required input parameters is six: two to define the initial disturbance, two for the deep-sea geometry, and two to describe the continental shelf. The initial disturbance of the free surface, η_d, at time $t = 0$, is given by

$$\eta_d(r,0) = \eta_0 e^{-(r/a)^2} \tag{1}$$

where (η_0, a) are the initial maximal amplitude and lateral extent of the disturbance, respectively, and r is the distance from the center of the initial disturbance (in the case of an underwater earthquake, the center will be located at the earthquake epicenter).

[6] Equation (1) describes an axisymmetric hump of water. The depth of the deep-sea H is assumed constant, and it extends from the center of the initial tsunami at $r = 0$ to the edge of the continental shelf at $r = L$. The depth h of the continental shelf is assumed to vary linearly according to

$$h(r) = \frac{(L + l - r)}{l} h_0, \qquad L \le r \le L + l \tag{2}$$

where (l, h_0) are the width and depth at the edge of the continental shelf, respectively. A crucial point in our approach is the distinct separation between the driving wave in deep water and the driven wave on the continental shelf. This separation is possible due to the step discontinuity, and is mathematically unjustified when $h_0 = H$. A schematic drawing of the flow domain is shown in Figure 1.

[7] The mathematical formulation and solution are outlined in section 2. The theoretical results of the idealized model for the deep sea and for the continental shelf are presented in sections 3 and 4, respectively. Comparisons with field measurements for the continental shelf and the deep sea are given in section 5 and Appendix B, respectively.

[8] Note that most of the tsunami sources are elongated rather than axisymmetric. Motivated by the task of developing a tool for generating synthetic tsunami databases, we

[1]Department of Civil and Environmental Engineering, Technion–Israel Institute of Technology, Haifa, Israel.

0148-0227/11/2010JC006763

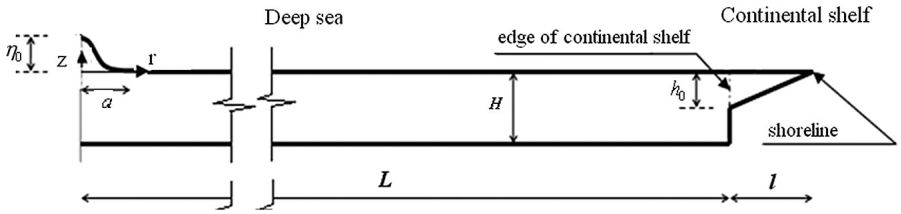

Figure 1. A schematic illustration of the flow domain.

tried to keep the number of source parameters as small as possible. The axisymmetric cases require three parameters: the epicenter, η_0, and a. On the other hand the elongated cases require two additional parameters: the length of the rupture area b and the orientation of the long axis, θ. In Appendix A we identify the cases for which the theoretical axisymmetric source provides a good approximation for actual elongated disturbances.

2. Mathematical Formulation and Solution

[9] The flow in deep sea is assumed to be inviscid, irrotational, axisymmetric, and thus governed by the axisymmetric Laplace equation:

$$\frac{1}{r}\frac{\partial}{\partial r}\left(r\frac{\partial \varphi}{\partial r}\right)+\frac{\partial^2 \varphi}{\partial z^2}=0, \qquad -H\le z\le 0,\ r\ge 0 \quad (3)$$

where $\varphi(r, t)$ is the velocity potential and z is the vertical coordinate. The bottom and linearized free surface boundary conditions are

$$\frac{\partial \varphi}{\partial z}=0, \qquad z=-H \quad (4)$$

and

$$\frac{\partial^2 \varphi}{\partial t^2}+g\frac{\partial \varphi}{\partial z}=0, \qquad z=0 \quad (5)$$

respectively, and g is the acceleration of gravity. The free surface elevation in deep sea $\eta_d(r, t)$ is related to φ through:

$$\eta_d=-\frac{1}{g}\frac{\partial \varphi}{\partial t} \quad (6)$$

[10] The problem defined in (3)–(6), together with the initial condition (1) constitutes the classical Cauchy-Poisson problem. The solution of this problem, which can be found in section 50 of *LeBlond and Mysak* [1978], is given by the integral:

$$\eta_d(r,t)=\frac{\eta_0 a^2}{2}\int_0^\infty k e^{-(ka)^2/4}J_0(kr)\cos(\Omega t)dk \quad (7)$$

In (7), J_0 is the zero-order Bessel function of the first kind, and the frequency Ω is related to the wavenumber k, through the linear dispersion relation:

$$\Omega^2=gk\tanh(kH) \quad (8)$$

[11] The evolution of the tsunami on the continental shelf is modeled by the one-dimensional linear shallow water equation; see equations (5.36) and (5.68) in the work of *Dean and Dalrymple* [1984]:

$$\frac{\partial^2 \eta_s}{\partial t^2}+A\frac{\partial \eta_s}{\partial t}=g\frac{\partial}{\partial r}\left(h\frac{\partial \eta_s}{\partial r}\right), \qquad L\le r\le L+l \quad (9)$$

[12] In (9), the water depth h is given by (2), η_s is the free surface elevation on the continental shelf, and A is a friction coefficient. The use of the rectangular one-dimensional equation (9) rather than its axisymmetric counterpart (for which the right-hand side of (9) would have the additional term $\frac{g}{r}\frac{\partial(h\eta_s)}{\partial r}$) is justified since L is assumed much larger than l.

[13] The solution of (9) is required to be finite at the shoreline, $r = L + l$, for all time and to be compatible to the deep-sea solution (7) at the edge of the continental shelf:

$$\eta_s(L,t)=\kappa_t \mathbf{H}(t)\eta_d(L,t) \quad (10)$$

In (10), $\mathbf{H}(t)$ is the Heaviside step function, and κ_t is the transmission coefficient of long waves over an abrupt depth change, from a depth of H to a depth of h_0, given by:

$$\kappa_t=\frac{2}{1+\sqrt{h_0/H}}, \quad (11)$$

See equation (5.55) in the work of *Dean and Dalrymple* [1984].

[14] The solution for the continental shelf region is obtained by using a Fourier transform from the time domain to frequency domain

$$\tilde{\eta}_s(r,\omega)=\frac{1}{\sqrt{2\pi}}\int_{-\infty}^{\infty}\eta_s(r,t)e^{-i\omega t}dt \quad (12a)$$

and its inverse

$$\eta_s(r,t)=\frac{1}{\sqrt{2\pi}}\int_{-\infty}^{\infty}\tilde{\eta}_s(r,t)e^{i\omega t}d\omega \quad (12b)$$

[15] Applying (12a) to equation (9) leads to a Bessel equation in r, with the solution:

$$\tilde{\eta}_s(r,\omega)=C_1J_0\left(2\sqrt{\frac{(\omega^2-i\omega A)l(L+l-r)}{gh_0}}\right)+C_2Y_0\left(2\sqrt{\frac{(\omega^2-i\omega A)l(L+l-r)}{gh_0}}\right), L\le r\le L+l \quad (13)$$

The boundness condition requires that $C_2 \equiv 0$, whereas the coefficient C_1 is obtained by substituting (13) into the Fourier transform of the boundary condition (10). These steps lead to:

$$\tilde{\eta}_s(r,\omega) = \frac{\kappa_t \eta_0 a^2}{4} B_0(r,\omega) \int_0^\infty dk \cdot k \cdot \exp\left(\frac{-(ka)^2}{4}\right) \cdot J_0(kL) \cdot \cdot \left[\sqrt{\frac{\pi}{2}}\delta(\omega-\Omega) + \sqrt{\frac{\pi}{2}}\delta(\omega+\Omega) - \frac{i}{\sqrt{2\pi}(\omega-\Omega)} - \frac{i}{\sqrt{2\pi}(\omega+\Omega)}\right] \quad (14)$$

where δ is the Dirac Delta function and

$$B_0(r,\omega) = \frac{J_0\left(2\sqrt{\frac{(\omega^2 - i\omega A) l (L+l-r)}{g h_0}}\right)}{J_0\left(2l\sqrt{\frac{(\omega^2 - i\omega A)}{g h_0}}\right)} \quad (14')$$

[16] Applying the inverse Fourier transform (12b) to (14) gives:

$$\eta_s(r,t) = \frac{\kappa_t \eta_0 a^2}{4} \int_0^\infty dk \cdot k \cdot \exp\left(\frac{-(ka)^2}{4}\right) J_0(kL) \cdot \left[\frac{e^{i\Omega t}}{2} B_0(r,\Omega) + \frac{e^{-i\Omega t}}{2} B_0(r,-\Omega) - Q(r,t,k)\right], \quad (15)$$

where

$$Q(r,t,k) = P.V \int_{-\infty}^{\infty} \frac{i}{2\pi} B_0(r,\omega) \cdot \left[\frac{1}{\omega-\Omega} + \frac{1}{\omega+\Omega}\right] e^{i\omega t} d\omega \quad (16)$$

The integrand in (16) has simple poles at $\omega = \pm\Omega$, and $\omega = \omega_j$, $j = 1,2,\ldots$, where

$$\omega_j = \frac{iA}{2} \pm \sqrt{\frac{g h_0 \alpha_j^2}{4l^2} - \frac{A^2}{4}}, \quad (17)$$

α_j are the positive zeros of J_0, i.e., $J_0(\alpha_j) = 0$ $\alpha_j > 0$.

[17] Applying the Cauchy residue theorem to (16) yields:

$$Q(r,t,k) = \begin{cases} \frac{e^{i\Omega t}}{2} B_0(r,\Omega) + c.c., & for \quad t < 0 \\ -\frac{e^{i\Omega t}}{2} B_0(r,\Omega) + \sum_{j=1}^{\infty} e^{-At/2} B_j(r,\Omega) + c.c, & for \quad t > 0 \end{cases} \quad (18)$$

where c.c. stands for the complex conjugate, and

$$B_j(r,\Omega) = \frac{g h_0 \alpha_j}{l^2 \sqrt{\frac{g h_0 \alpha_j^2}{l^2} - A^2}} \cdot \frac{J_0\left(\alpha_j \sqrt{\frac{L+l-r}{l}}\right)}{J_1(\alpha_j)} \cdot \exp\left(\frac{it}{2}\sqrt{\frac{g h_0 \alpha_j^2}{l^2} - A^2}\right) \cdot \left[\frac{1}{\sqrt{\frac{g h_0 \alpha_j^2}{l^2} - A^2} - 2\Omega + iA} + \frac{1}{\sqrt{\frac{g h_0 \alpha_j^2}{l^2} - A^2} + 2\Omega + iA}\right], \quad j = 1,2,\ldots \quad (19)$$

In (19), J_1 is the first-order Bessel function of the first kind. Substituting (18) into (15) reveals that $\eta_s(r, t) = 0$ for $t < 0$ and provides the final analytical step in our derivation, for $t \geq 0$.

[18] The integration over k in either (7) or (15) is carried out numerically using Matlab. The routine used, QUADGK, is based on the adaptive Gauss-Kronrod quadrature method and is recommended for calculation of oscillatory integrals. The routine supports infinite integration intervals on condition that the function value decays rapidly at infinity. QUADGK calculates the integrand value until reaching a relative tolerance error of 10^{-6}, this being the ratio of the tolerance error divided by the "exact" value. In addition, numerical experimentation revealed that setting the upper bound of the sum over j in (18), to 100, provides a stable result, for the cases examined.

[19] The energy loss over the continental shelf region has two main components, a loss due to bottom friction and a loss due to energy leaking back into deep sea. It turns out that the second component is significantly larger than the first. Using the reflection coefficient appropriate for waves propagating over a step from shallow to deep water, given in equation (5.56) of *Dean and Dalrymple* [1984]:

$$\kappa_r = \frac{\sqrt{H/h_0} - 1}{\sqrt{H/h_0} + 1} \quad (20)$$

and comparing it to the attenuation of progressive waves in water with an average depth of $h_0/2$, due to the effect of an "artificial" bottom friction A, over a distance of $2l$, given by: $\exp(-Al/\sqrt{0.5 g h_0})$, obtained from equations (5.78) and (5.80) of *Dean and Dalrymple* [1984], yields:

$$A = \sqrt{\frac{g h_0}{2}} \frac{\ln(\kappa_r^{-1})}{l} \quad (21)$$

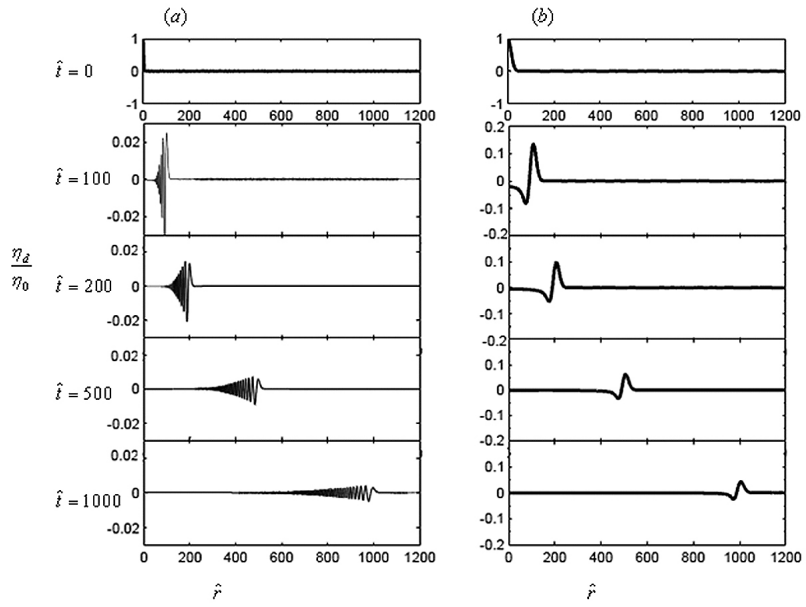

Figure 2. Tsunami evolution in deep sea: (a) wave packet, $\hat{a} = 3$, (b) single-wave, $\hat{a} = 20$.

For $h_0/H \ll 1$, (21) simplifies to:

$$A = \sqrt{\frac{2g}{H}}\frac{h_0}{l} \tag{22}$$

3. Results for the Deep Sea

[20] In this and in the following sections, dimensionless parameters are used:

$$\left(\hat{a}, \hat{r}, \hat{L}, \hat{l}, \hat{h}_0\right) = (a, r, L, l, h_0)/H \tag{23a}$$

and

$$\hat{t} = t\sqrt{g/H}\,, \hat{A} = A\sqrt{H/g} \tag{23b}$$

In Figure 2, two different cases of dimensionless a ($\hat{a}$ = 3, 20) are calculated to present the profound difference found between two types of tsunami in the deep sea. The graphs for η_d/η_0 are given as a function of $\hat{r}$and are derived from (7) for different instants in dimensionless time, i.e., $\hat{t}$ = 0,100,200,500, and 1000.

[21] The difference between the two cases is profound. The case with $\hat{a}$ = 3 corresponds to a dispersive wave packet, whereas the case $\hat{a}$ = 20 corresponds to a nondispersive single wave. The single-wave moves with the speed $\sqrt{gH}$ (dimensionless speed = 1), whereas the front of the wave packet moves somewhat slower than $\sqrt{gH}$.

[22] In order to provide a more general picture, two characteristic quantities are introduced. First, the tsunami amplitude, which is defined as the extreme deviation from the mean sea surface (either elevation or depression):

$$\hat{\eta}_{d,\max}(r) = \max|\eta_d(r,t)|/\eta_0 \tag{24a}$$

Second, the tsunami half period ($T_{1/2}$), which is defined as the time difference between the arrival of the above-

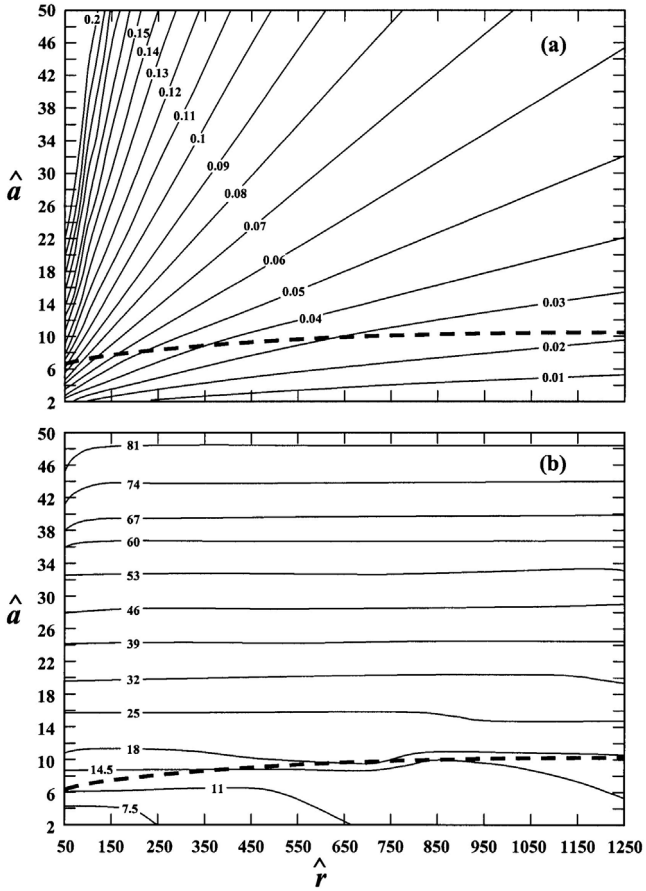

Figure 3. Contour lines for tsunami characteristics in deep sea as a function of $\hat{a}$and $\hat{r}$: (a) tsunami amplitude and (b) tsunami half period. Dashed lines separate between the single-wave cases (above the line) to the wave packet cases (below the line).

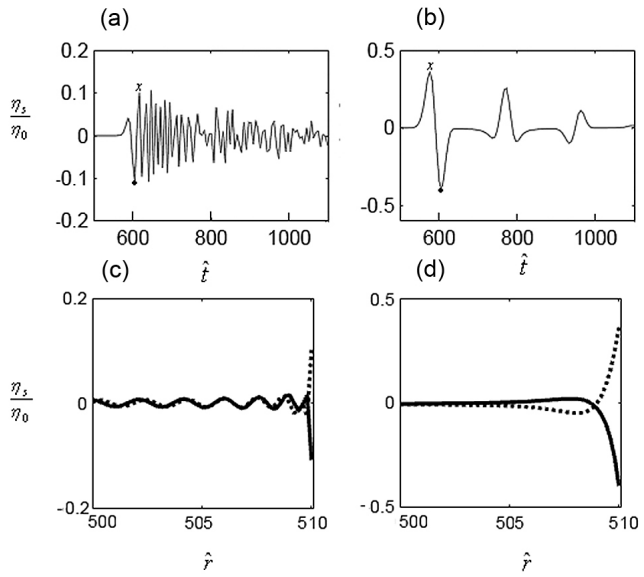

Figure 4. Tsunami evolution on the continental shelf for $\hat{L} = 500$, $\hat{l} = 10$, $\hat{h}_0 = 0.05$ ($\hat{A} = 0.007$). Temporal evolution at the shoreline for (a) $\hat{a} = 3$ (wave packet) and (b) $\hat{a} = 20$ (single-wave), respectively. (c,d) Spatial evolution along the shelf at the instants marked by dots and crosses on Figures 4a and 4b, respectively (dots, solid line; crosses, dashed line).

mentioned extreme, either crest or trough, to the arrival of the following trough or crest, respectively.

$$\hat{T}_{1/2} = T_{1/2}\sqrt{g/H} \tag{24b}$$

[23] Figure 3 gives the variation of tsunami amplitude $\hat{\eta}_{d,\max}$ and half period $\hat{T}_{1/2}$ as a function of $\hat{a}$and $\hat{r}$. The contour lines were calculated on the basis of 25 points in $\hat{r}$(50,100,…,1250), and 25 points in $\hat{a}$(2, 4,…,50). The dashed line is an attempt to separate the single-wave cases, for which $\hat{T}_{1/2}$ is almost independent of $\hat{r}$(above the dashed line), from the wave packet cases (bellow the dashed line).

[24] By comparing the volume of the original disturbance $\pi a^2\eta_0$ to the volume of a ring with radius $\hat{r}$ and a rectangular cross section with width $\hat{a}$and height $\hat{\eta}_{d,\max}$, one obtains:

$$\hat{\eta}_{d,\max} \approx \frac{\hat{a}}{2\hat{r}}, \qquad \hat{r} > \hat{a} \tag{25a}$$

which is in reasonable agreement with the results for a single-wave tsunami in Figure 3a. From Figure 3b one may find that for single-wave tsunamis:

$$\hat{T}_{1/2} \approx 1.5\hat{a} \tag{25b}$$

4. Results for the Continental Shelf

[25] Equation (15) is used to calculate the evolution of the tsunami on the continental shelf, for $\hat{L} = 500$, $\hat{l} = 10$ and $\hat{h}_0 = 0.05$, for which (21) gives $\hat{A} = 0.007$. The temporal evolution at the coastline of $\eta_s(L + l)/\eta_0$ for a wave packet tsunami ($\hat{a} = 3$) and a single-wave tsunami ($\hat{a} = 20$) are given in Figures 4a and 4b, respectively. The instants of extreme deviation from mean sea level are marked by a dot on Figures 4a and 4b. The crosses marked on Figures 4a and 4b correspond to the moment when the closest positive deviation occurs. Figures 4c and 4d show the spatial picture of the free surface across the continental shelf, i.e., η_s/η_0. The full line appearing in Figures 4c and 4d represents the spatial picture at the moment marked by a dot and the broken line the spatial picture at the moment marked by the cross. For both cases the extreme values appear at the shoreline.

[26] When comparing the results of Figure 4 to those of Figure 2 (for $\hat{r} = 500$, and $\hat{t} \approx 500$), one can see that the wave amplitudes at the shoreline are significantly larger than those at the edge of the continental shelf. Thus one may say that the continental shelf acts as a tsunami amplifier. In order to substantiate this statement, Figure 5 provides the values of the averaged ratios between the amplitude of $\eta_{s,\max}$ at the shoreline ($r = L + l$) and the amplitude of $\eta_{d,\max}$ just before the edge of the continental shelf ($r = L$), as a function of the continental shelf parameters $\hat{h}_0$ and $\hat{l}$.

[27] Thus an amplification factor is defined as

$$a_f = \overline{\eta_{s,\max}(L + l)/\eta_{d,\max}(L)} \tag{26}$$

where the bar denotes the averaging. Figure 5a is suitable for single-wave tsunamis, for which the averaging was done over nine cases: ($\hat{L}$, $\hat{a}$) = (200,20),(200,30),(200,50), (500,20),(500,30),(500,50), (1000,20),(1000,30),(1000,50).

[28] Figure 5b corresponds to wave packet tsunamis, for which the averaging was carried out over six cases: ($\hat{L}$, $\hat{a}$) = (200,3),(200,8),(500,3),(500,8),(1000,3),(1000,3). The six cases of wave packet tsunamis and nine cases of single-wave tsunamis were chosen to represent the geophysical range appropriate to tsunamis examined far from their source. Choosing more cases will consequently lead to a somewhat more detailed result. The number of cases for the wave packet tsunami is smaller due to the fact that the range of $\hat{a}$defining this wave type is much smaller than the range of $\hat{a}$defining the single-wave tsunami, as may be seen in Figure 3b.

[29] The continental shelf amplification factors reach values from 2.5 to 30 for the wave packet tsunamis and 2 to 11 for single-wave tsunamis. The difference in continental shelf amplification factors highlights another difference between the two tsunami wave types.

[30] The contour lines in Figure 5 are based on nine points in $\hat{l}$and nine points in $\hat{h}_0$. The standard deviation for wave packet and single-wave tsunamis are typically of the order of 10% and 20% of the average values, respectively. Note that the tsunami half period at the coastline $\hat{T}_{c.l}$ is rather similar to the half period at the edge of the continental shelf $\hat{T}_{c.s}$. In our calculations the ratio $\hat{T}_{c.l}/\hat{T}_{c.s}$ varied from 0.7 to 2.

5. Comparison With Measurements

[31] A comparison between the idealized model and deep-sea measurements is given in Appendix B. In this section we compare the coastal tsunami records measured at Male-Maldives and Pointe La-Rue-Seychelles, during the 26 December 2004 Sumatra-Andaman tsunami, with results of the idealized model. The recorded measurements were

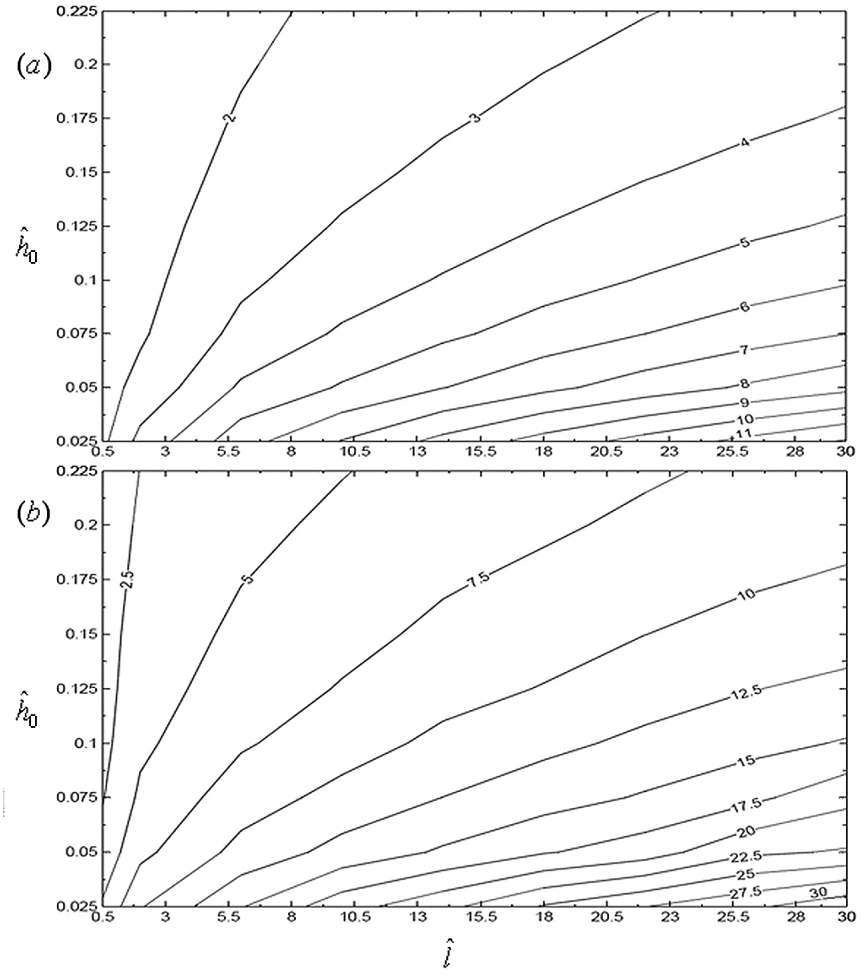

Figure 5. Contour lines for the continental shelf tsunami amplification factor a_f as a function of $\hat{h}_0$ and $\hat{l}$: (a) for single-wave cases and (b) for wave packet cases.

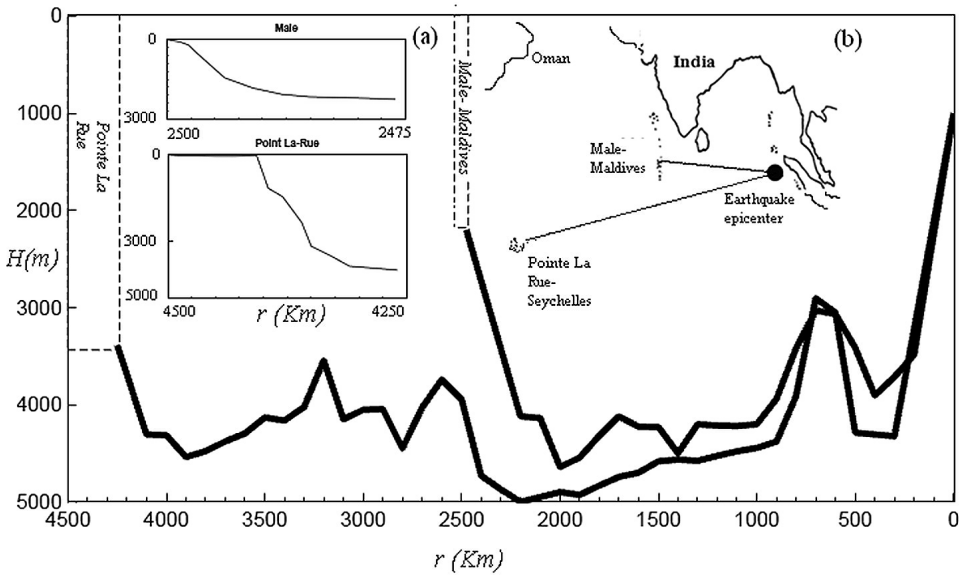

Figure 6. (a) The bathymetry in the vicinity of the continental shelf. (b) The bathymetry along the lines connecting the earthquake epicenter with Male-Maldives and Pointe La-Rue-Seychelles.

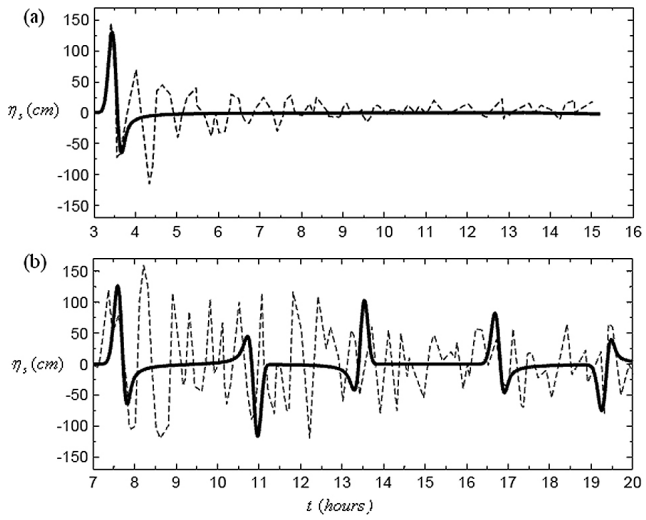

Figure 7. Temporal evolution of the free water surface at the shoreline of Male-Maldives and Pointe La-Rue-Seychelles during the Sumatra-Andaman tsunami (2004). The time t is measured from the instant of generation; solid line shows model results and dashed line shows tide gauge recording (University of Hawaii sea level center). List of parameters: $a = 101.5_{Km}$, $\eta_0 = 11.7_m$; (*a*) Male, $\overline{H} = 3970_m$, $l = 2.2_{Km}$, $h_0 = 200_m$,$A = 6.6 \cdot 10^{-3}$ $_{1/\mathrm{sec}}$, $L = 2500_{Km}$; (*b*) Pointe la Rue, $\overline{H} = 3875_m$, $l = 93_{Km}$, $h_0 = 35_m$,$A = 2.5 \cdot 10^{-5}$ $_{1/\mathrm{sec}}$, $L = 4500_{Km}$.

taken from the Web site of the University of Hawaii Sea Level Center (http://ilikai.soest.hawaii.edu/uhslc/iotd).

[32] The 2004 Sumatra-Andaman tsunami was caused by a submarine earthquake with a Moment Magnitude of 9.0 and an epicenter located at 3.307°N, 95.947°E (United States Geological Survey http://earthquke.usgs.gov/eqinthenews/2004/usslav/). The locations of the earthquake epicenter and of the tide gauge stations, as well as bathymetry along the lines which connect these two locations, are given in Figure 6b.

[33] A comparison between the measured free surface elevation by the tide gauge stations and that calculated from the model equation (15) is shown in Figures 7a and 7b for the Male-Maldives and Pointe La-Rue-Seychelles tide gauges, respectively. The six parameters required for the model calculation were estimated as follows:

[34] 1. The initial amplitude $\eta_0(m)$ and lateral extent $a(Km)$, were calculated using equations for slip displacement $D(m)$, and rupture area $\mathbf{A}(Km^2)$ given by *Wells* and *Coppersmith* [1994]:

$$\log_{10} D = 0.63M - 4.45 \tag{27a}$$

$$\log_{10} \mathbf{A} = 0.82M - 2.87 \tag{27b}$$

where M is the Moment Magnitude of the earthquake. The following assumptions give the relationship between the earthquake parameters given by *Wells and Coppersmith* [1994] and the tsunami parameters required for the model calculation:

$$\eta_0 = 0.7D \tag{28a}$$

assuming an average dip angle of about 45°, and

$$\pi a^2 = \mathbf{A} \tag{28b}$$

which is consistent with the lower bound of equation (2.3) in the work of *Levin and Nosov* [2009]. Using the Moment Magnitude provided by the United States Geological Survey, the tsunami parameters required for the model calculation, given by (27) and (28), are $\eta_0 = 11.7m$ and $a = 101.5Km$.

[35] 2. The deep sea parameters are the distance between the earthquake epicenter and the tide gauge location (for Male-Maldives, $L \approx 2500Km$ and for Pointe La-Rue-Seychelles, $L \approx 4500Km$), and the averaged depth $\overline{H}$ calculated from the deep sea depths, $H(r)$ by:

$$\overline{H} = \left[\frac{1}{L}\int_0^L \sqrt{H(r)}dr\right]^2 \tag{29}$$

giving $\overline{H} = 3970$ m and $\overline{H} = 3875$ m for Male-Maldives and Pointe La-Rue-Seychelles, respectively. The values of L and $H(r)$ were obtained from Google Earth (http://earth.google.com).

[36] 3. The continental shelf parameters were estimated from the bathymetry in the vicinity of the coastline (also taken from Google Earth), see Figure 6a, and the values chosen were $l = 2.2Km$, $h_0 = 200m$ for Male-Maldives and $l = 93Km$, $h_0 = 35m$ for Pointe La-Rue-Seychelles.

[37] From Figure 7 one may see that the model reproduces fairly well the time of tsunami arrival, its amplitude, and half period. The graph of the idealized model in Figure 7a decays rather fast and does not include the subsequent oscillations, which one may attribute to the excitation of edge waves (see *Mei et al.* [2005], section 12.4, on subharmonic resonance of edge waves excited by a normal incident wave on a slopping beach). Another possible source for this discrepancy could be the simplistic description of the initial elevation used herein.

6. Summary and Conclusions

[38] For the idealized configuration used herein, the calculations done by the simplified model provide the following picture:

[39] 1. For an axisymmetric source, the tsunamis in deep sea undergo a reduction in amplitude, according to Figure 3a, as they move away from the location of the tsunami source.

[40] 2. Continental shelves act as tsunami amplifiers. The present model produces tsunami amplitudes at the shoreline which are sometimes significantly larger than their values at the edge of the continental shelf (see Figure 5).

[41] 3. None of our many calculations of tsunamis generated far from the inspected shorelines produced an amplitude at the shoreline which was larger than double the initial tsunami amplitude, η_0. It is quite interesting to note that *Tinti and Tonini* [2005], who studied tsunamis generated close to the coastline, obtained a similar result.

[42] 4. The tsunamis may be split into two categories, a single-wave tsunami and a wave packet tsunami, with different properties for each of the wave types.

[43] 5. Single-wave tsunamis, which are obtained for $\hat{a} > 10$, are almost nondispersive. This is in contrast to wave

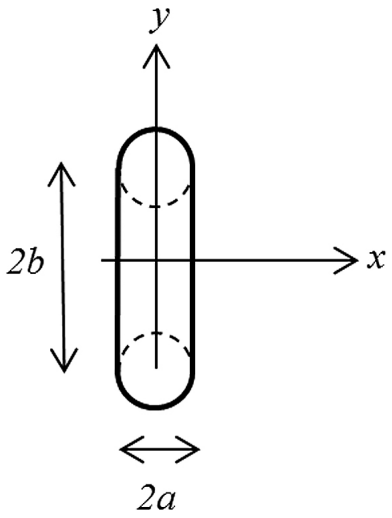

Figure A1. A schematic illustration of an elongated disturbance.

packet tsunamis for which dispersive effects play a more significant role.

[44] 6. When observing the earthquake equations provided by *Wells and Coppersmith* [1994], it may be concluded that for the formation of a significant tsunami at the shoreline, the Moment Magnitude of the earthquake must be at least 6.5, forming a tsunami belonging to the single-wave tsunami type. On the other hand, a volcano eruption, an under water landslide, and an underwater explosion [see *Le Méhauté*, 1971], in the vicinity of the continental shelf, may produce an initial wave with a relatively large amplitude (η_0) and a relatively small lateral extent, a, causing a large wave packet tsunami.

[45] 7. The tsunami amplitude at the coast and its half period seem to convey the most significant part of hydrodynamic information, for coastal engineering purposes.

[46] 8. The idealized model (which depends on six basic parameters, which may be collected with relatively little effort) produces the basic parameters required for calculating synthetic tsunami databases.

Appendix A: Elongated Disturbances

[47] Assuming an elongated tsunami source as shown in Figure A1, with typical length $2b$ and typical width $2a$, equations (1) and (7) are generalized to:

$$\eta_d(x,y,0) = \frac{\eta_0}{2b}\int_{-b}^{b} \exp\left\{-\left[x^2+(y-y_0)^2\right]/a^2\right\}dy_0 \qquad \text{(A1)}$$

and

$$\eta_d(x,y,t) = \frac{\eta_0 a^2}{4b}\int_0^\infty dk\cdot k\cdot e^{-(ka)^2/4}\cos(\Omega t)\int_{-b}^{b} dy_0 J_0 \cdot\left(k\sqrt{x^2+(y-y_0)^2}\right), \qquad \text{(A2)}$$

respectively. Expanding,

$$x^2+(y-y_0)^2 = x^2+y^2-2yy_0+y_0^2 = r^2-2yy_0+y_0^2 = r^2\left\{1-\frac{2yy_0-y_0^2}{r^2}\right\} \qquad \text{(A3)}$$

For $r \gg b$:

$$\sqrt{x^2+(y-y_0)^2} \approx r\left\{1-\frac{2yy_0-y_0^2}{2r^2}\right\} \qquad \text{(A4)}$$

[48] The main contribution to (A2) comes for the vicinity of $k = O(a^{-1})$. In addition we restrict the discussion to $y = O(b)$. Under these conditions:

$$k\frac{2yy_0-y_0^2}{2r} = O\left(b^2/ar\right) \qquad \text{(A5)}$$

The Taylor expansion of the term integrated over y_0 in (A2) is

$$J_0\left(k\sqrt{x^2+\left(y^2-y_0^2\right)}\right) = J_0(kr)+\frac{2yy_0-y_0^2}{2r}kJ_1(kr)+\ldots \qquad \text{(A6)}$$

Integration of (A6) by y_0 gives

$$\frac{1}{2b}\int_{-b}^{b}\left(J_0(kr)+\frac{2yy_0-y_0^2}{2r}kJ_1(kr)\right)dy_0 = J_0(kr)-\frac{kb^2}{6r}J_1(kr) = J_0(kr)+O\left(\frac{b^2}{ar}\right) \qquad \text{(A7)}$$

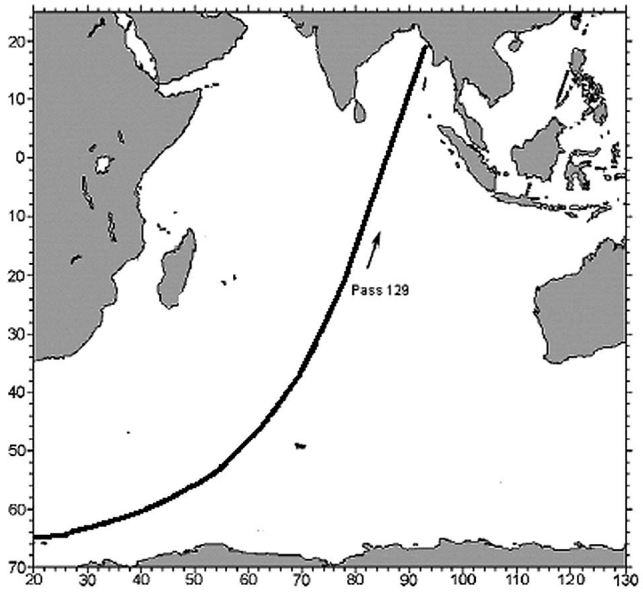

Figure B1. Pass 129 of Jason 1 altimeter taken on 26 December 2004 (based on Figure 1 in the work of *Gower* [2005]).

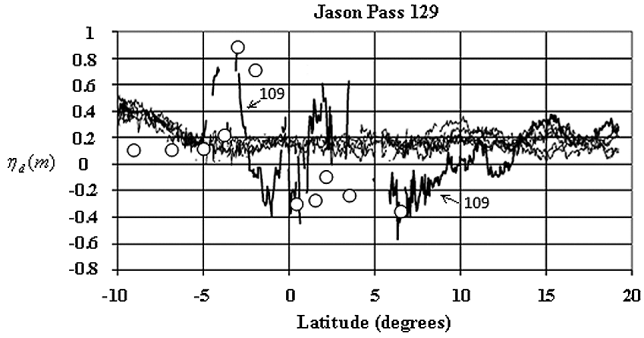

Figure B2. Water surface elevation along Pass 129. Cycle 109 gives the water surface elevation 2 h after the earthquake rupture. The open circles were calculated by the idealized model (based on Figure 2 in the work of *Gower* [2005]).

[49] Thus the leading order of (A2) reduces to (7), for $r \gg b$; i.e., for locations with large x/b but not too large y/b.

Appendix B: A Comparison Between Deep Sea Measurements by Jason 1 Satellite and the Idealized Model

[50] The model for the deep sea is compared to measurements by the satellite Jason 1, which measured the sea surface elevation 2 h after the moment of tsunami generation (see Figure B1). The method of parameter derivation for the idealized model was identical to that presented in section 5.

[51] The mean sea level, apparent from the measurements presented by *Gower* [2005], was 10 cm, and free surface elevation derived by the model (7) was adjusted accordingly. From Figure B2 one can see that the values calculated by the idealized model (given by open circles) agree quite well with measurements taken during Cycle 109.

[52] **Acknowledgments.** This research was supported by the Israel Science Foundation (grant 63/09) and by the Israel Ports Company. The research is part of a M.Sc. thesis submitted by J.T. to the Graduate School of the Technion–Israel Institute of Technology.

References

Constantin, A., and D. Henry (2009), Solitons and tsunamis, *J. Phys. Sci.*, *64*, 65–68.

Dean, R. G., and R. A. Dalrymple (1984), *Water Wave Mechanics for Engineers and Scientists*, World Sci., Singapore.

Gower, J. (2005), Jason 1 detects the 26 December 2004 tsunami, *Eos Trans. AGU*, *86*(4), 37–38, doi:10.1029/2005EO040002.

Hammack, J., and H. Segur (1978), The Korteweg-de Vries equation and water waves. Part 3. Oscillatory waves, *J. Fluid Mech.*, *84*(2), 337–358, doi:10.1017/S0022112078000208.

LeBlond, P. H., and L. A. Mysak (1978), *Waves in the Ocean*, Elsevier, New York.

Le Méhauté, B. (1971), Theory of explosion-generated water waves, in *Advances in Hydroscience*, vol. 7, edited by V. te Chow, pp. 1–79, Academic, New York.

Levin, B., and M. Nosov (2009), *Physics of Tsunamis*, Springer, Heidelberg, Germany.

Madsen, P. A., D. R. Fuhrman, and H. A. Schäffer (2008), On the solitary wave paradigm for tsunamis, *J. Geophys. Res.*, *113*, C12012, doi:10.1029/2008JC004932.

Mei, C. C., M. Stiassnie, and D. K.-P. Yue (2005), *Theory and Applications of Ocean Surface Waves*, World Sci., Singapore.

Tinti, S., and R. Tonini (2005), Analytical evolution of tsunamis induced by near-shore earthquakes on a constant-slope ocean, *J. Fluid Mech.*, *535*, 33–64, doi:10.1017/S0022112005004532.

Wells, D. L., and K. J. Coppersmith (1994), New empirical relationships among magnitude, rupture length, rupture width, rupture area, and surface displacement, *Bull. Seismol. Soc. Am.*, *84*, 974–1002.

M. Stiassnie and J. Tobias, Department of Civil and Environmental Engineering, Technion–Israel Institute of Technology, Haifa 32000, Israel. (miky@tx.technion.ac.il)